Tectonophysics xxx (2016) xxx–xxx

Contents lists available at ScienceDirect

Tectonophysics

journal homepage: www.elsevier.com/locate/tecto

Temperature and composition of carbonate cements record early structural control on cementation in a nascent deformation band fault zone: Moab Fault, Utah, USA

Keith R. Hodson *, Juliet G. Crider, Katharine W. Huntington

Department of Earth and Space Sciences, University of Washington, Seattle, WA 98195, USA

ARTICLE INFO

Article history:
Received 13 November 2015
Received in revised form 26 March 2016
Accepted 17 April 2016
Available online xxxx

Keywords:
Structural controls on fluid flow
Fault zone permeability
Carbonate clumped isotope thermometry
Deformation bands
Structural diagenesis

ABSTRACT

Fluid-driven cementation and diagenesis within fault zones can influence host rock permeability and rheology, affecting subsequent fluid migration and rock strength. However, there are few constraints on the feedbacks between diagenetic conditions and structural deformation. We investigate the cementation history of a fault-intersection zone on the Moab Fault, a well-studied fault system within the exhumed reservoir rocks of the Paradox Basin, Utah, USA. The fault zone hosts brittle structures recording different stages of deformation, including joints and two types of deformation bands. Using stable isotopes of carbon and oxygen, clumped isotope thermometry, and cathodoluminescence, we identify distinct source fluid compositions for the carbonate cements within the fault damage zone. Each source fluid is associated with different carbonate precipitation temperatures, luminescence characteristics, and styles of structural deformation. Luminescent carbonates appear to be derived from meteoric waters mixing with an organic-rich or magmatic carbon source. These cements have warm precipitation temperatures and are closely associated with jointing, capitalizing on increases in permeability associated with fracturing during faulting and subsequent exhumation. Earlier-formed non-luminescent carbonates have source fluid compositions similar to marine waters, low precipitation temperatures, and are closely associated with deformation bands. The deformation bands formed at shallow depths very early in the burial history, preconditioning the rock for fracturing and associated increases in permeability. Carbonate clumped isotope temperatures allow us to associate structural and diagenetic features with burial history, revealing that structural controls on fluid distribution are established early in the evolution of the host rock and fault zone, before the onset of major displacement.

1. Introduction

Rock permeability is strongly influenced by deformation, with major implications for the paths and rates of fluid migration through the upper crust. Diagenetic processes coupled with structural deformation can have complex feedbacks, further affecting structurally enhanced permeability, as well as rheological properties of rocks (e.g. Laubach et al., 2010). As such, characterization of these processes can inform geologic models of fault zone evolution and fluid migration. Porous sandstones are important reservoirs for geologic fluids in the upper crust, making characterization of the interplay between brittle deformation and diagenesis in these rocks particularly relevant to predictions of fluid migration and storage (e.g. Eichhubl et al., 2004; Laubach et al., 2010; Balsamo et al., 2013).

Joints and deformation bands (DBs) are two styles of deformation structures commonly observed in porous sandstones. Jointing refers to mode-I (opening) fracturing of the host rock, while DBs include a family of mm- to cm-thick tabular structures with a range of deformation mechanisms and kinematics, including dilation, compaction and shear (e.g. Aydin et al., 2006; Fossen et al., 2007). Dilation associated with jointing increases permeability of the host rock, creating conduits for fluid migration. Conversely, most types of DBs involve some degree of cataclasis, producing anastomosing zones of local grain size and porosity reduction (e.g. Aydin and Johnson, 1978; Antonellini et al., 1994). Some DBs are non-cataclastic, and may involve dilation and increases in permeability (e.g. Fossen et al., 2007). For cataclastic DBs, decreases in pore space can be quite substantial (e.g. Antonellini and Aydin, 1994; Eichhubl et al., 2009; Torabi et al., 2013) and have been commonly interpreted as an impedance to fluid flow (Knipe et al., 1997; Gibson, 1998). However, lateral outcrop-scale heterogeneities in DB zone continuity and thickness may diminish their effectiveness as barriers to fluid migration (e.g. Fossen and Bale, 2007). Furthermore, deformation bands may localize subsequent jointing (e.g. Tindall and Davis, 2003; Tindall and Eckert, 2015), enhancing cross-structure permeability (Tindall,

* Corresponding author at: Department of Earth and Space Sciences, University of Washington, Johnson Hall Rm-070, Box 351310, 4000 15th Avenue NE, Seattle, WA 98195-1310, USA.
E-mail address: krhodson@uw.edu (K.R. Hodson).

http://dx.doi.org/10.1016/j.tecto.2016.04.032
0040-1951/

2014). Some DBs also develop band-parallel fracture networks, which may enhance band-parallel permeability (e.g. Johansen et al., 2005).

Cementation along a fault zone is a record of fluid migration through fractures and pore space (e.g. Sample et al., 1993; Ohtani et al., 2000; Kirschner and Kennedy, 2001; Graham Wall et al., 2006; Balsamo et al., 2012, 2013), as well as a record of the source fluid chemistry (e.g. McCaig et al., 1995; Parry, 1998; Chan et al., 2000, 2001; Ghisetti et al., 2001; Shipton et al., 2004; Eichhubl et al., 2009). Stable isotope analysis of carbonate cement can be a particularly powerful tool, as bulk carbon and oxygen isotope ratios ($\delta^{13}C$ and $\delta^{18}O$, where δ indicates the relative abundance of the heavy isotope relative to a standard) are sensitive to source fluid composition, mineral formation temperature, and diagenetic processes (Mook, 1986; Kim and O'Neil, 1997). The "clumped isotope" (or Δ_{47}) composition of carbonate cement describes the abundance of carbonate ions containing both a heavy carbon and a heavy oxygen isotope (i.e., $^{13}C^{18}O^{16}O_2^{2-}$) relative to a stochastic distribution of isotopes. This isotope "clumping" is sensitive to temperature alone, and forms the basis of the carbonate clumped isotope paleothermometer (e.g. Ghosh et al., 2006; Schauble et al., 2006; Eiler, 2007, 2011). When conventional carbonate $\delta^{18}O$ measurements are paired with clumped isotope measurements, the relative influences of temperature and source-fluid composition on cement bulk isotope ratios can be determined. In the context of structural controls on fluid migration, paired temperature and source fluid composition provides insight into fault zone connectivity and thermal environments during cementation. When combined with micro-scale textural observations under polarized light and cathodoluminescence, the relative timing of cementation events during faulting, burial, and exhumation can be investigated (e.g. Loyd et al., 2012; Bergman et al., 2013; Budd et al., 2013; Huntington and Lechler, 2015).

Here, we use cements along the Moab Fault, southeast Utah, USA, to investigate the fluid migration history associated with the fault system. The surrounding Paradox Basin is interpreted to be an exhumed hydrocarbon system (e.g. Foxford et al., 1996; Nuccio and Condon, 1996), and the Moab Fault has hosted fluid migration within it. For this reason, the Moab Fault has been investigated by numerous workers interested in styles of structural deformation (e.g. Berg and Skar, 2005; Davatzes et al., 2005; Johansen et al., 2005) and their effects on fluid flow and associated carbonate cementation (e.g. Chan et al., 2000; Garden et al., 2001; Eichhubl et al., 2009; Bergman et al., 2013). Detailed mapping of structural (Davatzes et al., 2005; Johansen et al., 2005) and cementation patterns (Eichhubl et al., 2009) around a major fault-segment intersection along the Moab fault, referred to herein as Courthouse Junction (CHJ), provides an exceptional framework to investigate the interplay between structure and diagenetic cementation. We build upon earlier work at CHJ, using carbonate clumped isotope thermometry to identify relationships between carbonate cementation temperature, stable isotope composition, and structural history of the fault zone. Carbonate cementation at CHJ occurred during at least two discrete episodes, spanning a range of formation temperatures. Source fluids differed between episodes of cementation, including both marine and meteoric compositions. We connect the episodes of cementation to the stages of structural deformation along at CHJ, providing a view into fault zone development in conjunction with fluid-driven cementation and diagenesis, constrained by structural relationships, fluid temperature and stable isotopes. Deformation bands, formed at shallow depths, appear to precondition rock for fracturing, leading to increased fault parallel permeability early on in the rock burial history.

2. Geologic setting of the Moab Fault

The Moab Fault is a NNW trending, ~45 km-long, normal fault system within the Paradox Basin of southeast Utah, USA (Fig. 1). The fault offsets a package of Pennsylvanian to Cretaceous sedimentary strata, deposited in basins associated with the ancestral and modern Rocky Mountain orogenies (Foxford et al., 1996) and salt diapirism within the

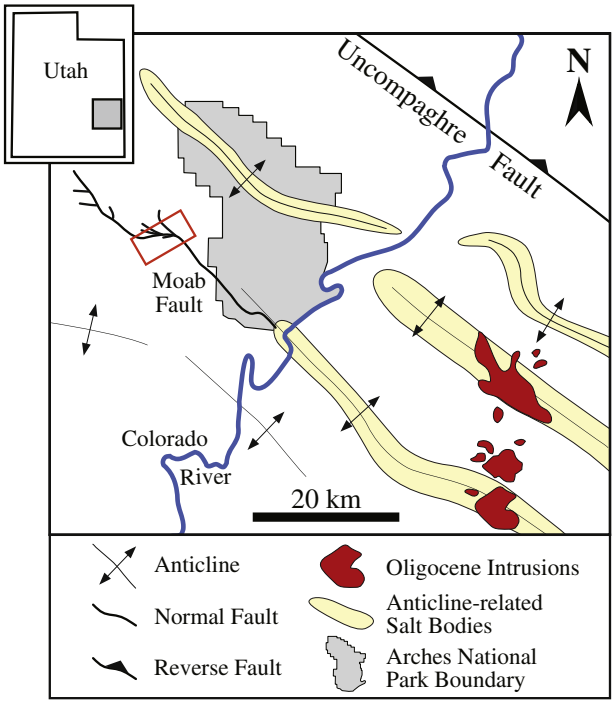

Fig. 1. Schematic regional map of Paradox Basin showing locations of major geologic features. Red box denotes location of Fig. 2. Yellow shapes mark locations of modern salt walls of the Paradox Formation. Red shapes mark locations of Oligocene La Sal laccolith intrusions. Map modified from Doelling (1985). (For interpretation of the references to color in this figure legend, the reader is referred to the web version of this article.)

Paradox Formation (Trudgill, 2011). Salt upwelling along the Moab Fault occurred throughout the Permian and Triassic (Trudgill, 2011). Dissolution of the Moab salt wall led to the eventual collapse of overlying strata (Gutiérrez, 2004), driving displacement along the Moab Fault beginning sometime after the late Triassic (Foxford et al., 1996; Trudgill, 2011). Fault throw has a maximum of ~1 km at the central portion of the southern segment, decreasing northwards to ~300 m near Courthouse Junction (Foxford et al., 1996). The main phase of slip accumulation is taken to be coeval with peak burial during the early Tertiary (Foxford et al., 1996; Nuccio and Condon, 1996), an interpretation that is supported by fault-gouge dates of 63 to 43 Ma (Pevear et al., 1997; Solum et al., 2005).

The main unit sampled in this study is the Jurassic Moab Tongue Member of the Curtis Formation (Doelling, 1985), a very well sorted, ~30 m thick, quartz sandstone. The unit is composed of eolian dunes and interdune sediments with 17–25% porosity in undamaged rock, decreasing to as low as 1% in deformation bands around the Moab Fault (Antonellini et al., 1994; Johansen et al., 2005; Eichhubl et al., 2009). Liesegang banding is common in the area surrounding the fault zone, likely associated with observed bleaching of hematite grain coatings (Chan et al., 2000; Garden et al., 2001; Eichhubl et al., 2009).

Courthouse Junction (CHJ) and Mill Canyon represent zones of structural complexity associated with the linkage of fault segments. At CHJ, concentrated deformation is exposed in a ~2 hectare surface of Moab Tongue sandstone within a prism bounded on two sides by fault segments M1 and M2 (Fig. 2). Mill Canyon is flanked by an extensional relay zone in segment M2 to the east, and another major fault segment intersection to the west. Detailed structural mapping of exposures at CHJ and Mill Canyon by previous workers identified four classes of deformation structures, including joints, two types of cataclastic deformation bands, and jointed deformation bands (Figs. 3 and 4; Davatzes et al., 2005; Johansen et al., 2005). The styles of deformation band are distinguishable in outcrop by their widths, termed "thick" and "thin" by Johansen et al. (2005). Thick deformation bands (DBk) contain

Please cite this article as: Hodson, K.R., et al., Temperature and composition of carbonate cements record early structural control on cementation in a nascent deformation band faul..., Tectonophysics (2016), http://dx.doi.org/10.1016/j.tecto.2016.04.032

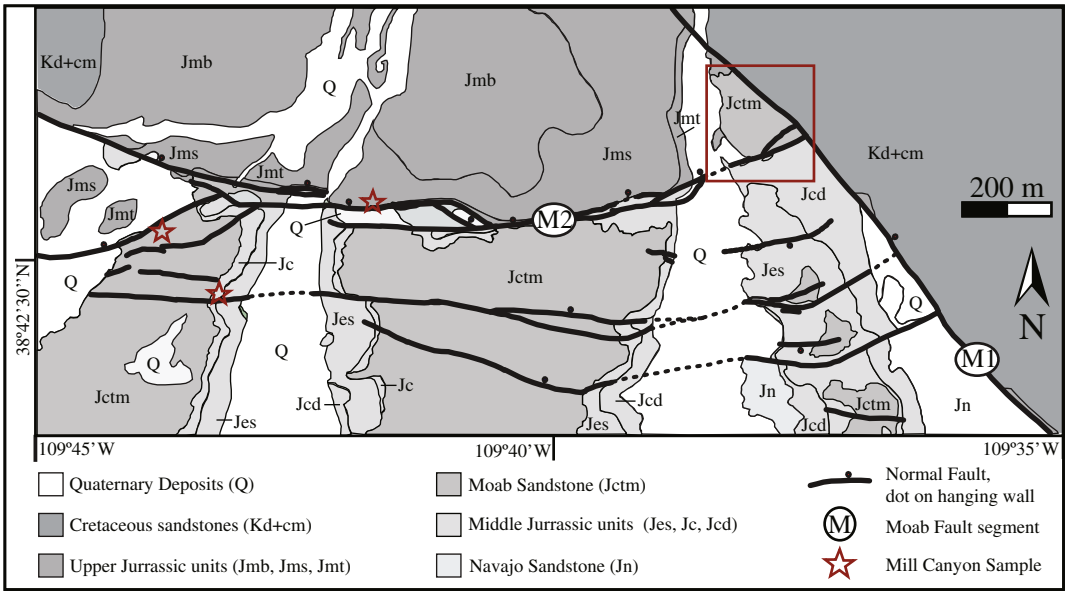

Fig. 2. Geologic map of Courthouse Junction and Mill Canyon. Red box denotes location of Courthouse Junction sandstone pavement and the majority of discussed samples (Fig. 7). Red stars mark locations of samples from Mill Canyon. Map modified from Davatzes et al. (2005). (For interpretation of the references to color in this figure legend, the reader is referred to the web version of this article.)

limited cataclasis, with crushed grains occupying spaces between undeformed grains. Thin deformation bands (DBn) appear in thin section as discrete, narrow zones with intense comminution. (We use the last letter of "thick" and "thin" in the abbreviations, because the initial letters are the same.) Johansen et al. (2005) observed that DBn cross-cut DBk, interpreting the change in DB style to reflect changes in confining pressures and rock stiffness associated with burial and quartz diagenesis. DBn accommodate subsequent shear along joints formed within and adjacent to the zones of intense grain-size reduction, and the joints were subsequently filled by carbonate cement.

Both quartz and carbonate cements are present within the Moab Tongue sandstone at CHJ and Mill Canyon (Eichhubl et al., 2009) and

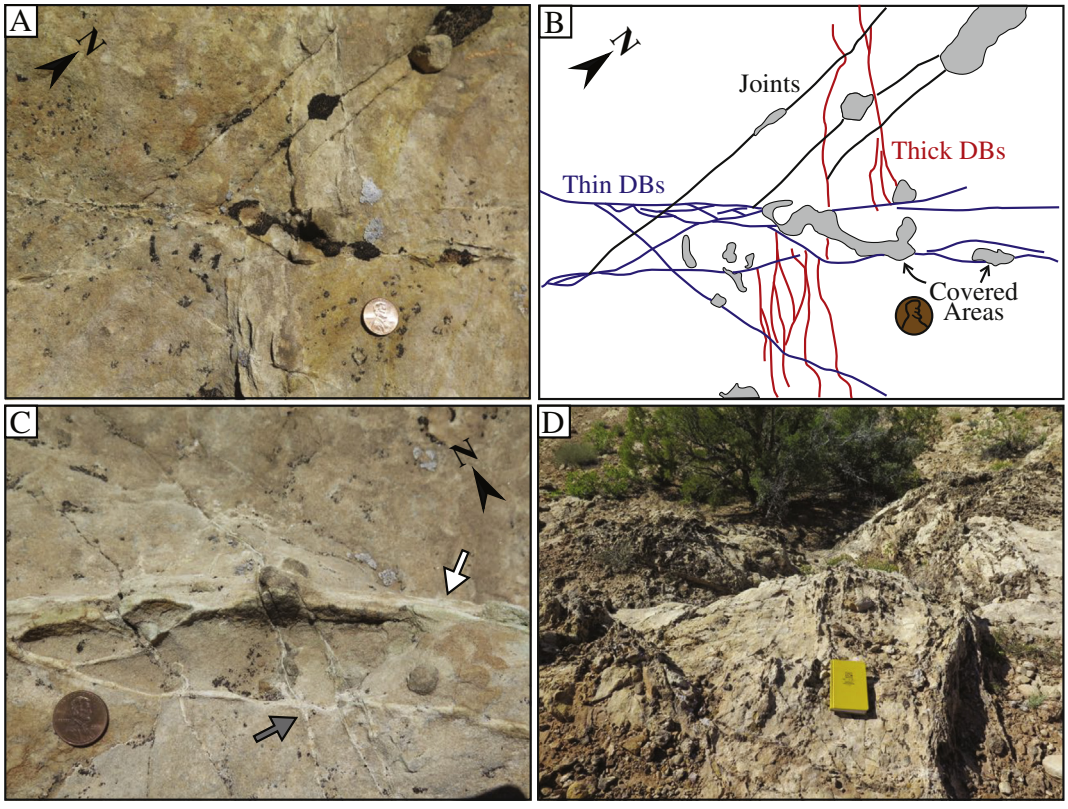

Fig. 3. Photographs of outcrops at Courthouse Junction. A) Three styles of brittle structures showing relative age. Coin is 19 mm in diameter. B) Line drawing of structures shown in A. Early thick deformation bands (red lines) are offset by thin deformation bands (blue lines), and both are cross cut by joints (black lines). C) Thick deformation bands (white arrow) cross cut by later thin deformation bands featuring thin carbonate veins (gray arrow). D) View to north across dense array of veins and concretions close to fault segment M2 (see Fig. 7 for location). Field notebook is 24 cm, long dimension. (For interpretation of the references to color in this figure legend, the reader is referred to the web version of this article.)

Please cite this article as: Hodson, K.R., et al., Temperature and composition of carbonate cements record early structural control on cementation in a nascent deformation band faul..., Tectonophysics (2016), http://dx.doi.org/10.1016/j.tecto.2016.04.032

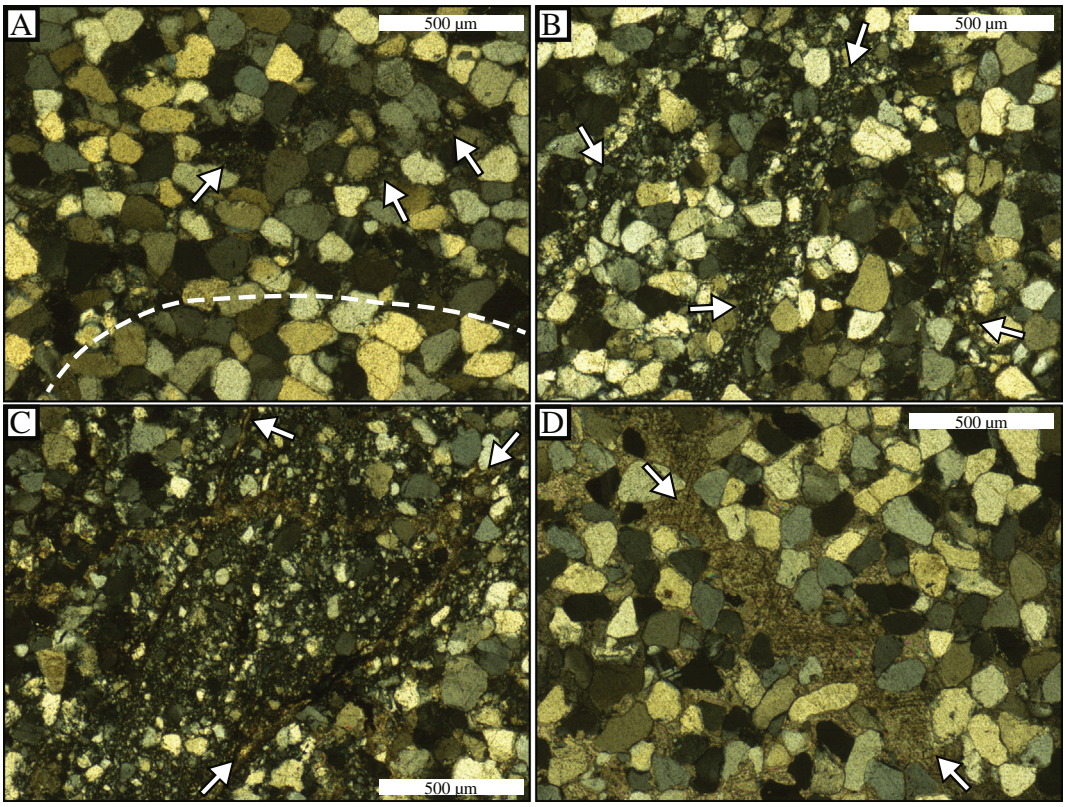

Fig. 4. Plane light photomicrographs displaying the four main classes of structures at Courthouse Junction. A) Thick deformation band associated with notable quartz pressure solution. White arrows denote locations with localized grain crushing and carbonate cementation. Dashed white line marks approximate edge of deformation band. B) Thin deformation bands (white arrows) in compacted host rock. C) Fractured zone of thin deformation bands filled by carbonate veins (white arrows). D) Vein filling joint not associated with deformation band (arrows).

elsewhere along the Moab fault (Chan et al., 2000; Garden et al., 2001). Eichhubl et al. (2009) noted that some joints are only partially filled by carbonate, concluding that the carbonate fills formed within an open joint network. Stable isotope and fluid inclusion studies from this part of the Moab Fault showed that carbonate cements have a range of isotope compositions, suggesting at least two different fluid sources for the cements, with at least one in conjunction with hydrocarbons (Chan et al., 2000; Garden et al., 2001; Eichhubl et al., 2009; Bergman et al., 2013). Clumped isotope thermometry identified cements that precipitated at warm and cool temperatures, with apparent structural control on the relative distribution of the two fluids (Bergman et al., 2013). We evaluate these relationships by combining clumped isotope measurements with microstructure observations, placing each carbonate into context with the known burial history and evolving style of structural deformation at CHJ and Mill Canyon.

3. Sample collection and characterization

We collected samples for bulk and clumped stable isotope analyses and thin section analysis. The samples were selected to provide both broad spatial coverage across CHJ and to represent the range of cementation styles associated with the four classes of deformation structures documented at CHJ and Mill Canyon: thick and thin deformation bands, jointed thin deformation bands, and joints not related to deformation bands.

Thin sections were prepared from 59 sandstone samples. Petrographic observations were made using a standard transmitted-light microscope and a Luminoscope ELM-3R cold-cathode catholuminescence stage (operated between 5 and 10 kV, ~0.5 mA, 50–100 mTorr), attached to a polarizing microscope fitted with an Olympus UC50 digital camera. We characterized cements in thin section based on their textural relationships to the four classes of deformation structures and by their luminescence. These observations were used to screen a subset for clumped isotope analysis, targeting samples exclusively containing either non-luminescent or luminescent carbonate.

4. Stable isotope methodology

Prior to analysis, hand samples were cut or broken to isolate carbonate associated with particular features of interest identified in thin section and hand sample, and then ground using an agate mortar and pestle. Large carbonate features were separated from the host rock before grinding. Given the mass of calcite needed for clumped isotope analysis (6–8 mg pure calcite equivalent per replicate), carbonate from thin veins or pore-filling cements was ground and homogenized with host rock with a bulk volume sufficient to yield the necessary mass of carbonate. Samples with paired observations of cathodoluminescence were taken from the same structures characterized in thin section.

All stable isotope analyses were performed at IsoLab at the University of Washington. Bulk carbon and oxygen isotope analyses ($\delta^{13}C$ and $\delta^{18}O$) were made using a Kiel III Device connected to a Thermo Scientific Delta Plus isotope ratio mass spectrometer using the methods of Tobin et al. (2011). Internal laboratory standards calibrated against NBS-18 and NBS-19 (IAEA, Vienna, Austria), and LSVEC (NIST, Gaithersburg, MD, USA) international standards were analyzed along with sample carbonates and used to convert measured isotope ratios to the Vienna Pee Dee Belemnite (VPDB) and Vienna Standard Marine Ocean Water (VSMOW) reference scales.

Samples for clumped isotope analysis (Δ_{47}) were first reacted with phosphoric acid at 90 °C, and the resultant CO_2 was prepared on an automated vacuum line following methods of Burgener et al. (2016). Details are provided in the supplementary materials. Purified gasses were then transferred to flame sealed glass tubes and stored until analysis on a dedicated Thermo MAT 253 isotope ratio mass spectrometer

Please cite this article as: Hodson, K.R., et al., Temperature and composition of carbonate cements record early structural control on cementation in a nascent deformation band faul..., Tectonophysics (2016), http://dx.doi.org/10.1016/j.tecto.2016.04.032

configured to measure m/z 44–49 (inclusive). Values for Δ_{47} were calculated using established methods (Huntington et al., 2009), and are reported in the absolute reference frame (Dennis et al., 2011) without a 25 °C correction for acid fractionation.

Values of Δ_{47} were converted to temperatures ($T\Delta_{47}$) using the calibration of Kluge et al. (2015; their Eq. 5). Since the introduction of carbonate clumped isotope thermometry (Ghosh et al., 2006; Eiler, 2007), a number of calibrations have been proposed linking Δ_{47} measurements to temperature (e.g. Ghosh et al., 2006; Guo et al., 2009; Dennis and Schrag, 2010; Eagle et al., 2010; Zaarur et al., 2013; Kluge et al., 2015). Differences among these calibrations are topics of ongoing research (e.g. Defliese et al., 2015; Kluge et al., 2015; Tripati et al., 2015). The calibration of Kluge et al. (2015) was chosen because it is the most recent version using materials and procedures most similar to our own: inorganic calcite and an elevated acid digestion temperature (90 °C). Differences in the slopes and intercepts of published calibration curves produce differences in $T\Delta_{47}$, and a graphical comparison of the two most used calibrations is provided in the supplementary materials. Because our findings are based principally on textural relationships and relative temperature, the interpretations presented are largely independent of our choice of calibration curve. A range of carbonate species has been observed at CHJ (e.g. calcite, ankerite, malachite), but because calcium carbonate speciation is not believed to significantly affect clumped isotope results (Defliese et al., 2015), we did not screen samples for mineralogy prior to analysis.

Simultaneous measurements of sample $\delta^{13}C$ and $\delta^{18}O$ made for each clumped isotope analysis were converted to VPDB and VSMOW reference scales using three internal laboratory standards calibrated to the NBS-18, NBS-19, and LSVEC international standards. For all but one sample, two to three replicate analyses were performed. Errors in $\delta^{13}C$, $\delta^{18}O$, temperature and derived fluid $\delta^{18}O$ values were determined using either the standard error of replicate sample analyses or the standard error of internal standards measured during the corresponding analysis period, whichever was larger.

5. Results

5.1. Textural relationships

All four types of structures described by Johansen et al. (2005) were identified in outcrop at Courthouse Junction and Mill Canyon (Fig. 3). We observed the same cross-cutting relationships between these structures described by Johansen et al. (2005) and Davatzes et al. (2005), progressing from early thick deformation bands to thin deformation bands, followed by development of joints and thin veins in the cores of DBn, and finally to the formation of joints and veins not associated with deformation bands.

Thick deformation bands (DBk) appear in thin section as zones of porosity reduction associated with pockets of crushed quartz grains and carbonate cement (Fig. 4A), analogous to the shear enhanced compaction bands of Eichhubl et al. (2010). As compared to thin deformation bands (DBn) that form discrete ribbons of cataclasis (Fig. 4B), DBk are less distinct in thin section. Carbonate cements associated with DBk appear to be concentrated within the zones of grain-size reduction. DBn can contain opening mode I microfractures in and along their cores, with smaller fractures commonly bridging larger through-going fractures (Fig. 4B and C). Carbonate fills these joints to form thin veins (Fig. 4C), suggesting that cement formation spanned the development of both DBk and DBn. Late stage joints are generally filled by mm to cm wide syntaxial veins composed of blocky crystalline carbonate cement. Joint-filling calcite is commonly twinned, which we interpret to indicate some amount of strain accumulation after cementation (Fig. 4D).

Cathodoluminescence (CL) reveals the presence of both luminescent and non-luminescent carbonate cement, both of which are present as pore-filling cements and within fractures (Fig. 5). Non-luminescent carbonate is typically finely crystalline, but also can have a reddish-brown, cloudy appearance in thin section under plane and polarized light (Fig. 5C, white arrow). Jointed DBn commonly contain non-luminescent carbonate cement. Non-luminescent carbonate also occurs as pore filling cement surrounding both DBn and DBk. Coarsely crystalline luminescent cement was observed filling late forming joints and infiltrating pore space in the surrounding host rock (Fig. 5). Patches of DBn material can be observed along the margins of some luminescent veins, indicating that the luminescent cement also filled jointed DBn. Centimeter-scale spherical concretions within the host rock and cement halos along joints consistently contain luminescent cements.

A range of brightness was observed in luminescent cements, from a dim reddish orange to bright orange. Because CL emissions are primarily controlled by the carbonate's trace element composition (Boggs and Krinsley, 2006), these variations in luminescence suggest some variability in source fluid chemistry during the formation of luminescent veins and pore-filling cements. Some veins display clear CL zonation along sharp boundaries that do not correspond to current grain boundaries (Fig. 5H), which in conjunction with observed mechanical twinning indicates recrystallization after deposition. Other luminescent veins have irregular boundaries between zones with differing CL brightness (Fig. 5D), suggesting that successive phases of cementation partially dissolved and replaced earlier cements.

Quartz grains in the analyzed samples commonly exhibit signs of compaction and pressure solution in the form of interlocking grains and quartz overgrowths (Fig. 4). Both luminescent and non-luminescent carbonate cements can be observed filling areas between previously interpenetrating grains, indicating cements with both CL characteristics formed after compaction (Fig. 5J shows a luminescent example). Some veins contain quartz grains suspended within the carbonate fill, such as the clastic dike described by Eichhubl et al. (2009) in the wall of Mill Canyon west of CHJ.

The relative age of luminescent and non-luminescent carbonate cements varies from sample to sample. First, non-luminescent cement that *predates* luminescent cement is observed both (1) as an earlier pore filling cement crosscut by later luminescent cement (Fig. 5A and B) and (2) along the margins of veins filled with younger luminescent carbonate (Fig. 5C and D). These veins can contain patches of comminuted grains along their margins, in the same style as DBn. The non-luminescent cements in this setting predate the luminescent vein fills, but must post-date the formation of DBn. Second, non-luminescent cement that *postdates* luminescent cement is also observed; non-luminescent cement occurs at the center of luminescent veins, filling fractures that crosscut earlier CL zonation (Fig. 5H). It seems that precipitation of non-luminescent cements occurred both before and after precipitation of the luminescent cements. We do not observe carbonate veins with alternating zones of luminescent and non-luminescent carbonate, nor have we found examples of mutual crosscutting in the same sample, suggesting that the phases of cementation did not overlap in time.

5.2. Stable isotope geochemistry

5.2.1. Bulk isotope measurements

We measured bulk carbon and oxygen stable isotope compositions on 31 individual samples (Table 1). Measured $\delta^{13}C$ values range from −5.2 to 4.0‰ VPDB, and measured $\delta^{18}O$ values range from −23.5 to 2.8‰ VPDB. $\delta^{13}C$ and $\delta^{18}O$ are positively correlated (Fig. 6A), similar to relationships described in earlier work at CHJ (Chan et al., 2000; Eichhubl et al., 2009; Bergman et al., 2013).

For a subset of samples, we have paired CL observations and isotope measurements. These analyses show that luminescent and non-luminescent carbonate cements have distinct $\delta^{13}C$ and $\delta^{18}O$ values (Fig. 6A). Samples containing luminescent carbonate have $\delta^{13}C$ values between −4.5 and −2.3‰ VPDB, and $\delta^{18}O$ values between −20.9 and −15.8‰ VPDB. Samples containing non-luminescent carbonate

Please cite this article as: Hodson, K.R., et al., Temperature and composition of carbonate cements record early structural control on cementation in a nascent deformation band faul..., Tectonophysics (2016), http://dx.doi.org/10.1016/j.tecto.2016.04.032

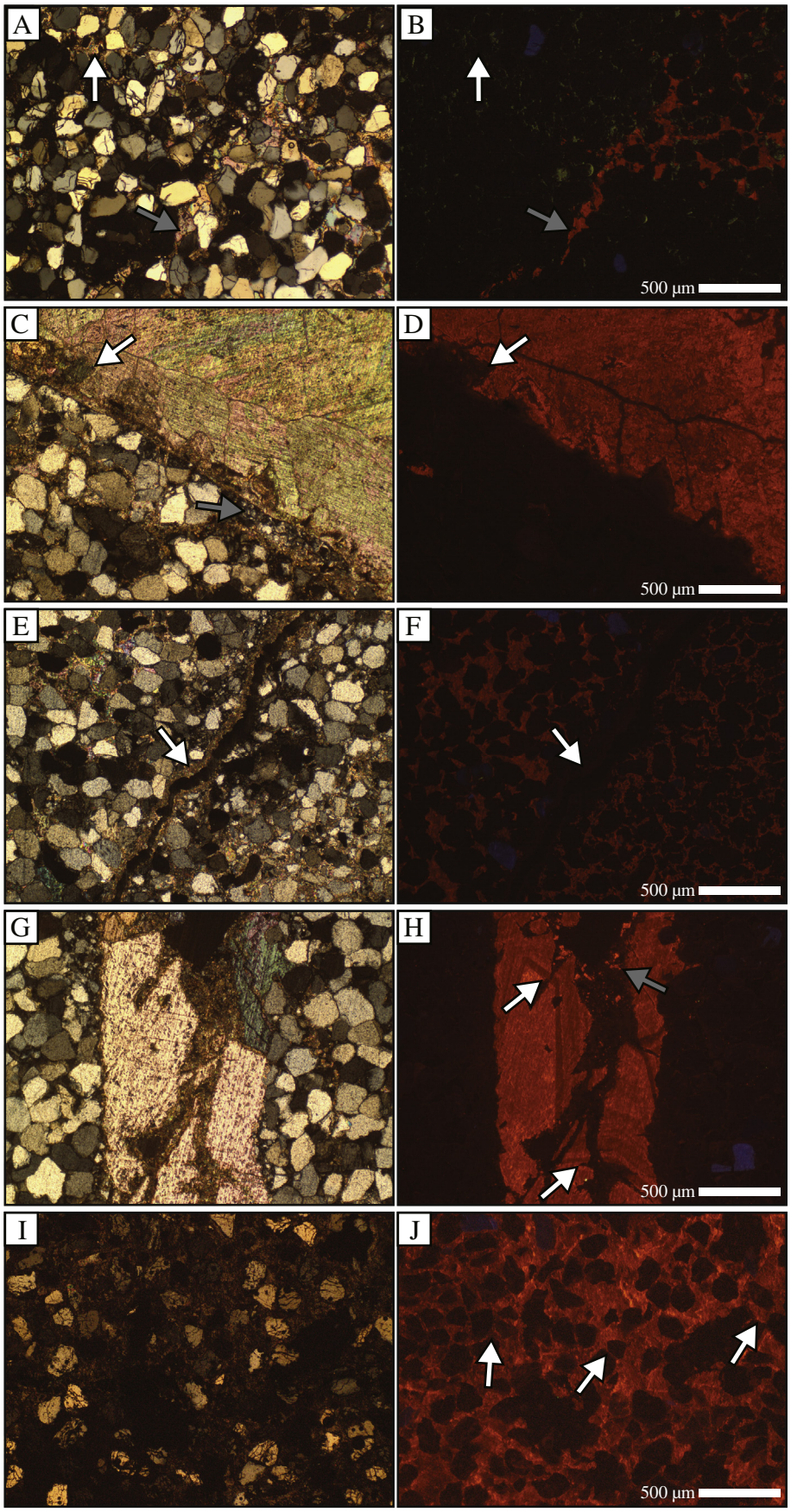

Please cite this article as: Hodson, K.R., et al., Temperature and composition of carbonate cements record early structural control on cementation in a nascent deformation band faul..., Tectonophysics (2016), http://dx.doi.org/10.1016/j.tecto.2016.04.032

have higher $\delta^{13}C$ values between −0.7 and 3.2‰ VPDB, and higher $\delta^{18}O$ values between −5.0 and −0.1‰ VPDB.

5.2.2. Carbonate clumped isotope thermometry

Out of the pool of samples with bulk isotope measurements, twenty-five samples were analyzed for clumped isotope thermometry (Table 1). For all but one sample (MCC15-KH05), reported values of Δ_{47} represent averages of 2 to 3 repeat measurements from the same sample. Sample average Δ_{47} values range from 0.505 to 0.681‰, corresponding to carbonate precipitation temperatures ($T\Delta_{47}$) of 7 °C to 73 °C (calibration of Kluge et al., 2015). Reported errors are the standard error for multiple replicate analyses from each sample or the long term standard deviation of an internal laboratory standard (1SD = 0.025‰) divided by the square root of the number of sample replicate analyses, whichever is larger. This produces sample specific uncertainty in $T\Delta_{47}$ between 4 and 14 °C (1SE, average of 6.8 °C)

Clumped isotope temperatures vary systematically with calcite luminescence, with non-luminescent carbonate yielding cool $T\Delta_{47}$ values (<18 °C), and luminescent carbonate showing higher $T\Delta_{47}$ values (>18 °C). Analyzed samples for which CL observations were not made have $T\Delta_{47}$ up to ~73 °C; bulk C and O isotopic compositions of these samples suggest that they likely belong to the luminescent group (Fig. 6A). Using the temperature dependence of oxygen isotope fractionation between carbonate and water determined by Kim and O'Neil (1997), calculated parent fluid $\delta^{18}O$ values are between −16 and −13‰ VSMOW for luminescent carbonate, but higher for non-luminescent carbonate: −6 and 0‰ VSMOW (Fig. 6C). Errors in these values, based on standard error in measured temperatures, fall between 1 and 3‰.

6. Discussion

The observation of strong correlations between carbonate $\delta^{18}O$ and $\delta^{13}C$ values, carbonate luminescence, carbonate precipitation temperature, and source fluid $\delta^{18}O$ values supports the interpretation that chemically and thermally distinct source fluids circulated at CHJ and Mill Canyon. The apparent association of luminescent and non-luminescent carbonate with different styles of structural deformation indicates that different source fluids are associated with different stages of structural deformation and the burial history. In the following discussion, we synthesize our findings with the known geologic history of the Moab Fault and Paradox Basin, providing constraints on the fluid sources for carbonate cement, the relative timing of cementation and structural deformation, and the thermal environments during burial and faulting.

6.1. Fluid sources

As outlined in Section 5.2.1, bulk isotope data delineate two end-member carbonate cement compositions (Fig. 6A). Earlier studies identified similar ranges in oxygen and carbon isotope compositions at CHJ (Chan et al., 2000; Eichhubl et al., 2009), and $\delta^{13}C$ values as low as −15‰ have been reported from further south along the Moab Fault system (Garden et al., 2001). CL observations support the conclusion of two end-member compositions at CHJ, as luminescent carbonates have consistently lower $\delta^{13}C$ and $\delta^{18}O$ values than non-luminescent carbonate (Fig. 6A). Inclusion of bulk isotope data from Bergman et al. (2013) with our results shows a continuous range of values between known luminescent and non-luminescent samples (Fig. 6). Known luminescent samples have relatively low bulk isotopic compositions and known non-luminescent samples have relatively high bulk isotopic compositions. This suggests that most of the observed spread can be attributed to the presence of both end-member carbonates within single samples at scales finer than the sample size.

Source fluid $\delta^{18}O$ values determined using $T\Delta_{47}$ also support the presence of two distinct end-member fluids. For our samples with known luminescence characteristics, there are two distinct source fluid $\delta^{18}O$ values: luminescent carbonate source fluids average approximately −13.5‰ and non-luminescent carbonate source fluids average approximately −3.3‰. Other source fluid $\delta^{18}O$ values from this study and Bergman et al. (2013), re-calculated using the temperature calibration of Kluge et al., 2015) fall between the end-members (Fig. 6), supporting the interpretation that many samples contain a mixture of luminescent and non-luminescent carbonate with these end-member isotopic compositions. Bergman et al. (2013) report one exception to this pattern: a non-luminescent sample with a source fluid $\delta^{18}O$ value of −13‰.

Considering that equilibrium fractionation of carbon between solid and dissolved carbonate is minor (~1‰; Mook, 1986), our data highlight approximate isotopic compositions for the source fluids and their dissolved inorganic carbon (DIC) content: a $\delta^{18}O$ value of −13.5‰ VSMOW and $\delta^{13}C$ value of −3.2‰ VPDB for luminescent carbonate and a $\delta^{18}O$ value of −3.3‰ VSMOW and $\delta^{13}C$ value of 1.3‰ VPDB for non-luminescent carbonate (Fig. 6d). Through the application of clumped carbonate thermometry, we confirm the suggestions of earlier studies at CHJ, identifying fluids with distinct isotopic compositions that produced the observed carbonate cements (Chan et al., 2000; Eichhubl et al., 2009; Bergman et al., 2013). Isotopic evidence for fluid sources has been discussed at length in earlier studies at CHJ and the surrounding region (Chan et al., 2000; Garden et al., 2001; Shipton et al., 2004; Crossey et al., 2009; Eichhubl et al., 2009; Dale et al., 2014), and we use our new data to evaluate the range of possible sources.

6.1.1. Possible carbon sources

Possible carbon sources for carbonate cements include marine waters, organic matter derived from plants, soil CO_2 from plant respiration, reduction of hydrocarbons, and magmatic degassing. Marine carbonates typically have $\delta^{13}C$ values between 0 and 4‰ VPDB (Shackleton, 1986), while $\delta^{13}C$ values between −30 and −20‰ VPDB are more typical of the latter three sources, although substantial enrichment in ^{13}C can occur due to complex microbial reactions (e.g. Irwin et al., 1977). Magmatic CO_2 typically has $\delta^{13}C$ values between −7 and −1‰ VPDB (e.g. Crossey et al., 2009; Hilton et al., 2010; Lucic et al., 2015).

Non-luminescent carbonates have $\delta^{13}C$ values within the range expected for a marine bicarbonate source. This follows the conclusion of Eichhubl et al. (2009) who attribute relatively high $\delta^{13}C$ values to marine DIC. The marine carbon could be derived from infiltrating marine waters as the Paradox Basin became flooded during the mid-Cretaceous (Trudgill, 2011), or could be from deeply circulating waters rich in dissolved limestone from Pennsylvanian, Permian, or Jurassic strata (Fig. 6A; Garden et al., 2001). Alternatively, modern CO_2-charged geysers and springs in the nearby Salt Wash Graben produce large surficial carbonate deposits with enriched $\delta^{13}C$ values (~4 to 8‰ VPDB; Fig. 6A; Shipton et al., 2004), and may be modern analogs for the formation of non-luminescent carbonate. Bacterial fermentation of organic carbon in the methanogenic zone (e.g. Dale et al., 2014; Irwin et al., 1977) is another possibility, predicted to produce $\delta^{13}C$ values between ~0 and 15‰.

Fig. 5. Paired plane light and cathodoluminescence (CL) photomicrographs demonstrating styles of carbonate luminescence and relative age. Exposure time for CL images is 1 s. A,B) Early non-luminescent pore-filling cement cross cut by later luminescent vein and pore-filling cement. White arrow points to pocket of non-luminescent cement in both images. Gray arrow marks luminescent vein. C,D) Early non-luminescent cement with later luminescent cement. White arrows point to boundary between luminescent and non-luminescent carbonate in both images. Gray arrow denotes pocket of thin deformation band material that predates both vein fills. E,F) Early luminescent pore-filling cement and later non-luminescent cement forming along margins of fracture. Arrow marks edge of non-luminescent cement in both images. G,H) Fractured luminescent vein filled by later non-luminescent cement. Zonation in CL is crosscut by non-luminescent cement (white arrows). Gray arrow denotes luminescent material entrained in later vein. I,J) Cement-supported quartz grains. Cement runs between previously interlocking grains (white arrows).

Please cite this article as: Hodson, K.R., et al., Temperature and composition of carbonate cements record early structural control on cementation in a nascent deformation band faul..., Tectonophysics (2016), http://dx.doi.org/10.1016/j.tecto.2016.04.032

Table 1
Stable isotopic data for carbonate cements.

Sample name	Sample location[a]		$\delta^{13}C$ (‰, VPDB)	$\delta^{18}O$ (‰, VPDB)	Δ_{47}		Temperature[e]			$\delta^{18}O$ fluid[f]		
	Latitude	Longitude			(‰, ARF)[b]	Stderr (‰)[c]	n[d]	(°C)	Stderr (°C)	(‰, VSMOW)	StdErr (‰)	Luminescent?[g]
CHJ14_JC02	38.71185	−109.73044	−3.1	−21.4	–	–	–	–	–	–	–	–
CHJ14_JC03	38.71176	−109.73006	3.3	2.8	0.62094	0.00429	3	25.5	5.0	5.3	1.0	–
CHJ14_JC04	38.71170	−109.73010	3.3	2.3	0.63298	0.01573	2	21.7	5.9	4.0	1.2	–
CHJ14_JC05	38.71172	−109.73000	−3.6	−20.9	0.52399	0.00932	3	63.7	7.2	−11.7	1.2	–
CHJ14_JC06	38.71135	−109.72953	−3.6	−21.7	–	–	–	–	–	–	–	–
CHJ14_JC07	38.71110	−109.72924	−3.9	−9.6	0.65462	0.00735	2	7.3	6.1	−11.0	1.4	–
CHJ14_JC08	38.71116	−109.72928	−2.8	−16.7	0.58935	0.00896	3	36.5	5.5	−12.2	1.0	–
CHJ14_JC09	38.71121	−109.72938	4.0	1.9	0.67006	0.01058	3	10.6	4.2	1.2	1.0	–
CHJ14_KH01	38.71136	−109.73106	−3.3	−23.5	0.52333	0.00865	2	66.4	9.1	−13.9	1.4	–
CHJ14_KH02	38.71134	−109.73105	−3.1	−22.5	0.50711	0.01528	3	71.9	7.7	−12.1	1.2	–
CHJ14_KH03	38.71113	−109.73080	−4.0	−22.9	–	–	–	–	–	–	–	–
CHJ14_KH04	38.71094	−109.73061	−3.4	−22.2	0.50910	0.00846	2	56.0	14.0	−14.3	2.4	–
CHJ14_KH05	38.71066	−109.73036	−4.2	−13.8	0.54983	0.01114	3	52.1	4.7	−6.5	0.8	–
CHJ14_KH06	38.71072	−109.73036	−3.9	−22.4	–	–	–	–	–	–	–	–
CHJ14_KH07A	38.71074	−109.73031	−4.1	−23.0	–	–	–	–	–	–	–	–
CHJ14_KH08	38.71061	−109.73034	−4.6	−22.6	0.50536	0.00855	3	72.8	7.8	−12.0	1.2	–
CHJ14_KH09	38.71069	−109.73042	−5.2	−19.9	0.54238	0.00886	3	55.3	6.6	−12.1	1.1	–
CHJ14_M2A	38.71134	−109.72923	1.9	−5.6	0.64805	0.00753	3	17.0	4.5	−4.9	1.0	–
CHJ14_M2B	38.71134	−109.72923	1.1	−5.3	–	–	–	–	–	–	–	–
CHJ15-KH02	38.71183	−109.73029	3.2	−0.1	0.67127	0.00394	2	10.2	5.2	−0.8	1.2	N
CHJ15-KH03	38.71180	−109.73026	−0.7	−5.0	0.66042	0.01713	2	13.3	5.4	−5.1	1.2	N
CHJ15-KH07	38.71152	−109.73081	1.5	−4.2	0.66712	0.01926	2	11.4	5.5	−4.7	1.2	N
CHJ15-KH08	38.71154	−109.73081	−3.5	−20.9	0.54579	0.00473	2	53.8	8.1	−13.3	1.4	Y
CHJ15-KH17	38.71113	−109.72922	−2.4	−16.2	0.61203	0.01017	2	28.5	6.3	−13.1	1.3	Y
CHJ15-KH18	38.71093	−109.72971	−4.5	−19.3	0.54756	0.00931	3	53.1	7.6	−11.8	1.3	Y
CHJ15-KH23	38.71083	−109.73007	0.8	−3.9	0.64768	0.01273	2	17.1	5.6	−3.1	1.2	N
CHJ15-KH24	38.71083	−109.73007	−3.2	−16.9	0.58915	0.01114	2	36.6	6.8	−12.3	1.3	–
CHJ15-KH24B	38.71083	−109.73007	−3.5	−18.5	0.56587	0.00794	2	32.9	11.9	−14.7	2.4	Y
MCC15-KH05	38.70916	−109.73871	1.4	−3.3	0.67280	0.00847	1	9.8	7.4	−4.1	1.7	N
MCE15-KH06	38.70742	−109.74565	2.0	−0.7	0.68110	0.00225	2	7.5	5.1	−2.1	1.2	N
MCE15-KH07	38.70743	−109.74580	−2.3	−15.8	0.64288	0.00034	2	18.6	5.7	−14.8	1.2	Y

[a] Sample location recorded with handheld GPS with nominal 5 m accuracy.
[b] Δ_{47} values calculated using the standard equations (Huntington et al., 2009) without an acid fractionation factor.
[c] Standard errors are from replicate analyses or long term variation of internal standards, whichever is larger.
[d] Number of replicate isotope analyses.
[e] Temperatures calculated using Eq. 5 of Kluge et al. (2015). Errors calculated using propagated Δ_{47} error.
[f] Source fluid $\delta^{18}O$ values calculated following the methods of Kim and O'Neil (1997). Errors propagated from error in calculated temperature.
[g] Observations of CL characteristics were made for a subset of samples prior to isotopic analysis.

Luminescent carbonate $\delta^{13}C$ values are below the typical range of marine DIC, but much higher than typical values for organic sources. Carbon sources for luminescent carbonate may have involved anoxic methanogenesis of organic acids, which can produce $\delta^{13}C$ values less than ~−4‰ (Baedecker et al., 1993), as suggested by Eichhubl et al. (2009), or thermocatalytic decarboxylation of organic carbon ($\delta^{13}C$ less than ~−3‰; Irwin et al., 1977), as was suggested by Dale et al. (2014) for concretions with similar $\delta^{13}C$ values in the Piceance basin ~50 km to the northeast of CHJ. Abundant spherical concretions at CHJ hint at microbe-assisted cementation, but $T\Delta_{47}$ shows that only half of the luminescent carbonates fall in the methanogenic temperature range (below ~40 °C; Irwin et al., 1977). The remaining luminescent carbonates have higher temperatures, consistent with thermal decomposition. Magmatic CO_2 associated with the intrusion of Oligocene Colorado Plateau laccoliths (Nelson et al., 1992) was determined by Crossey et al. (2009) to have $\delta^{13}C$ values between −9 and −3‰ VPDB, making waters charged with magmatic DIC another possible carbon source.

6.1.2. Possible oxygen sources

Non-luminescent carbonates have $\delta^{18}O$ values similar to, but lower than modern (~0‰ VSMOW) and Cretaceous (~1.2‰ VSMOW; Shackleton and Kennett, 1975) ocean waters. This may suggest a mixed marine and meteoric oxygen source for non-luminescent carbonate. Carbonate associated with modern CO_2-charged geysers, which have similar $\delta^{13}C$ values to non-luminescent carbonates, have $\delta^{18}O$ values between ~−9 and −12‰ VPDB (Shipton et al., 2004), somewhat lower than non-luminescent carbonates, which might be attributable to differences in carbonate precipitation temperature or degassing of CO_2.

The source fluids associated with luminescent, relatively warm carbonates have $\delta^{18}O$ values around −13.5‰ VSMOW, within the range of $\delta^{18}O$ values from modern meteoric water (−15 to −12‰; Spangler et al., 1996). While we do not necessarily expect modern and Mesozoic meteoric water to be equivalent, the similarity suggests a primarily meteoric source for the oxygen in the luminescent carbonates. A similar conclusion was reached by earlier interpretations of carbonate $\delta^{18}O$ values from CHJ (Chan et al., 2000; Eichhubl et al., 2009).

6.1.3. Source fluids at Courthouse Junction

Our new CL observations, structural observations, and chemical analyses allow us to describe the source fluids associated with the three stages of carbonate cements at CHJ. Measured non-luminescent carbonates have source fluids with $\delta^{18}O$ and $\delta^{13}C$ values similar to marine water and marine DIC. The association of early non-luminescent cements with the earliest deformation structures (DBk), cool $T\Delta_{47}$, and marine fluids suggests that these cements likely precipitated from intraformational marine waters during the earliest stages of diagenesis.

Luminescent carbonates are associated with joints, have warm $T\Delta_{47}$, and $\delta^{18}O$ within the expected range of meteoric water, consistent with deeply circulating basin water upwelling within the fault damage zone. The presence of warm meteoric waters, with associated carbonate temperatures reaching predicted ambient conditions during peak burial (Garden et al., 2001), follows the general framework proposed by Chan et al. (2000) and Eichhubl et al. (2009), where a carbon-rich, reducing fluid derived from hydrocarbons mixed with formation waters to form the (warm) carbonate cements. The presence of hydrocarbon residues

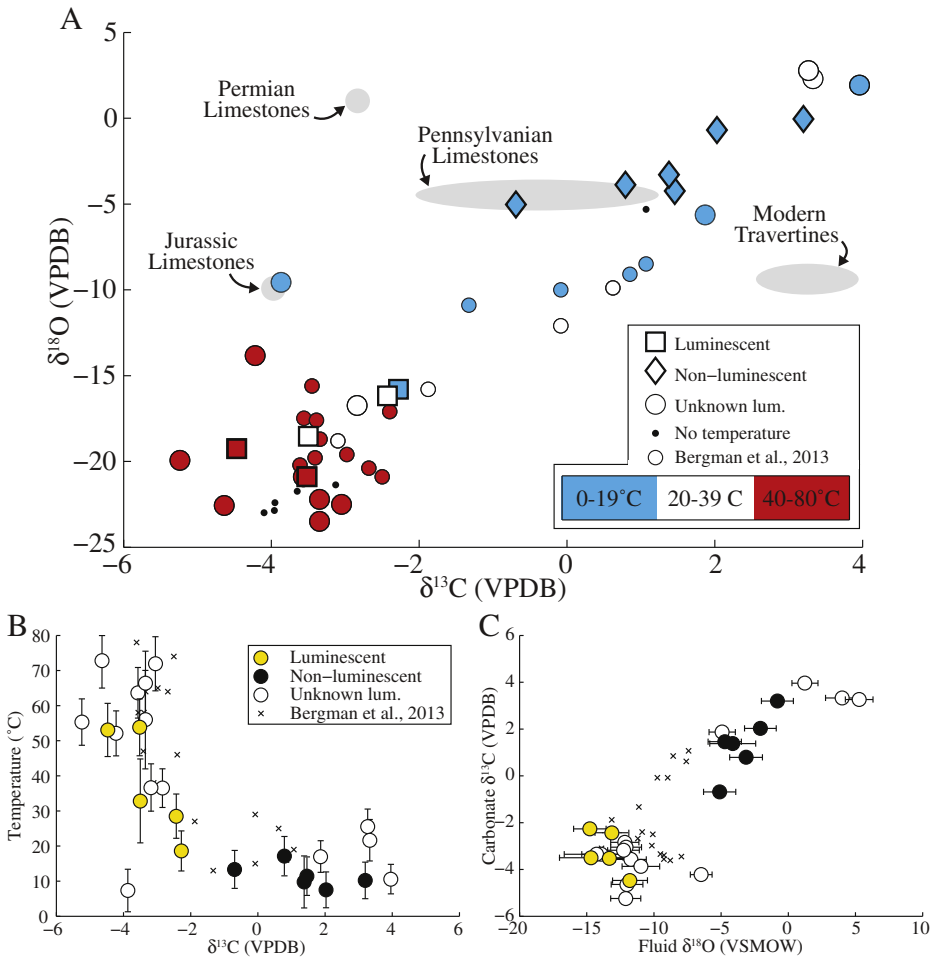

Fig. 6. Carbonate and source fluid chemistry. A) Carbonate stable isotope compositions colored by relative temperature. Blue to white transition occurs at 20 °C, corresponding to the break in temperature between luminescent and non-luminescent cements. White to red transition occurs at 40 °C, corresponding to approximate upper boundary for methanogenesis. Squares and diamonds denote samples known to be luminescent and non-luminescent under CL, respectively. Large circles indicate samples with unknown luminescence and small circles denote samples from Bergman et al. (2013), recalculated using the clumped isotope calibration of Kluge et al. (2015). Black dots denote samples without temperature measurements. Shaded fields outline approximate ranges of compositions for possible source fluids (Garden et al., 2001; Shipton et al., 2004). B) Carbonate precipitation temperature and $\delta^{13}C$ composition for samples with known luminescence characteristics (orange and black circles), unknown luminescence (white circles), and data from Bergman et al. (2013; black x's). C) Carbonate $\delta^{13}C$ and calculated source fluid $\delta^{18}O$ composition. Symbols as in B. Error bars denote standard error of replicate analyses. (For interpretation of the references to color in this figure legend, the reader is referred to the web version of this article.)

within the Moab Fault Zone supports the interpretation that degraded hydrocarbons yielded the observed $\delta^{13}C$ values, but our data cannot rule out magmatic CO_2 as a possible carbon source.

Source fluids for late non-luminescent carbonate remain ambiguous. Because they are difficult to isolate from luminescent cement during sampling, we do not have isotopic analysis from non-luminescent samples with clear a cross-cutting relationship showing late relative age. Bergman et al. (2103) report a single non-luminescent specimen with a meteoric oxygen isotope signature and a cool $T\Delta_{47}$. That specimen and the specimen shown in Fig. 5H (with late non-luminescent carbonate) are both from the intensely deformed damage zone near the fault (e.g. Fig. 3D). These observations support the interpretation that the high permeability damage zone served as a conduit for cool meteoric fluids (Bergman et al., 2013) or was active following exhumation to near-surface depths (Fig 8, box C).

6.2. Thermal and structural context for carbonate deposition

Cool, non-luminescent cements are observed within DBk and jointed DBn, as well as in fractures cross-cutting warm, luminescent cements. Luminescent cements are found within joints as well as jointed DBn. By combining the established sequence of structural deformation (DBk, DBn, jointing of DBn, and jointing not associated with DBs) with the relative ages and contrasting temperatures of cool, non-luminescent and warm, luminescent cements, we can place the coupled structural and diagenetic history of the Moab sandstone at CHJ into the broader context of basin evolution and deformation on the Moab Fault (Fig. 8).

Growth of the Moab Salt Wall ended by the late Triassic (Trudgill, 2011). The Moab Tongue sandstone was deposited last in a series of Jurassic eolian sandstones, marking the transition to the deposition of lacustrine and fluvial sediments (Trudgill, 2011). Catacastic DBs have been previously observed in shallowly buried sediments (e.g. Cashman and Cashman, 2000), so shallow burial of a weakly cemented Moab Tongue sandstone could have driven development of early DBk (Fig. 8). Preferential carbonate cementation within DBk suggests some structural control on fluid distribution, possibly due to a transient increase in porosity associated with dilation prior to cataclasis (e.g. Bésuelle, 2001; Fossen et al., 2007). The cool $T\Delta_{47}$ of these cements are consistent with near-surface temperatures, further supporting the shallow formation of associated deformation bands.

Continuing burial during the early Cretaceous (Fig. 8) increased temperatures and confining pressures, driving quartz pressure solution and overgrowth cementation (Johansen et al., 2005). Associated porosity reduction and stiffening of the rock triggered a change in deformation mechanism to produce the thinner, more intensely cataclastic DBn.

Please cite this article as: Hodson, K.R., et al., Temperature and composition of carbonate cements record early structural control on cementation in a nascent deformation band faul..., Tectonophysics (2016), http://dx.doi.org/10.1016/j.tecto.2016.04.032

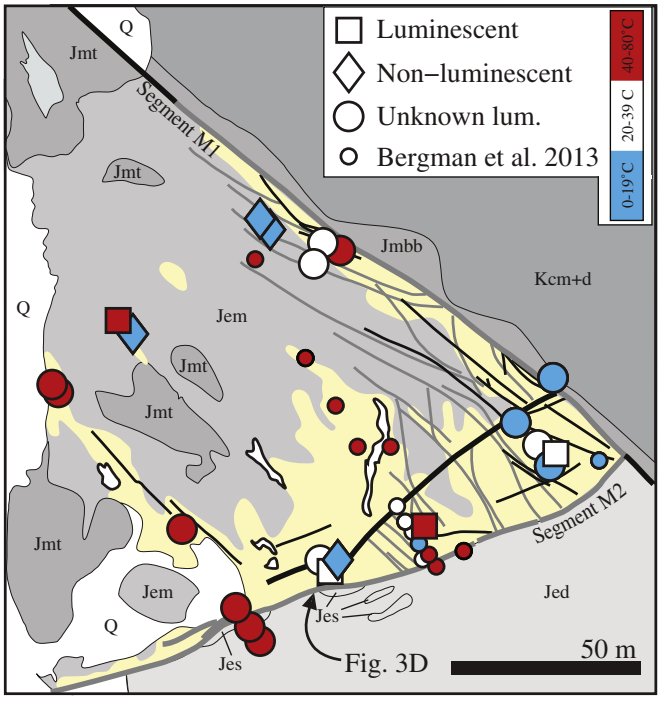

Fig. 7. Detail map of CHJ outcrop, showing sample locations and distribution of clumped isotope temperatures in relation to major structures. Color scale and symbols as in Fig. 6A. Thick black and gray lines are major deformation band- and joint-based faults, respectively. Thin black and gray lines are prominent deformation bands and joints, respectively.
Yellow shading denotes extent of carbonate cementation after Eichhubl et al. (2009). Structures as mapped by Davatzes et al. (2005); map modified from Eichhubl et al. (2009). (For interpretation of the references to color in this figure legend, the reader is referred to the web version of this article.)

Subsequently, joints developed in DBn, due to increased differential stress from either rapid burial during the mid- to late-Cretaceous or early episodes of faulting, and these became filled with additional cool, non-luminescent cement. The cool $T\Delta_{47}$ suggests that the formation and fracturing of DBn also occurred at shallow depths.

As the Moab Tongue sandstone reached peak burial depths of ~2 km and temperatures of ~60 to 80 °C (Fig. 8; also Garden et al., 2001), the main phase of faulting along the Moab Fault generated new pathways for fluid migration along the fault zone. Local fluid overpressure (Garden et al., 2001) and stresses associated with faulting (Davatzes et al., 2005) produced a joint network cross-cutting the jointed DBn, further enhancing permeability around the fault. Warm, reducing fluids migrated up from below (Garden et al., 2001), mixed with meteoric formation waters and precipitated the warm, luminescent carbonate cements in existing joints (Chan et al., 2000; Eichhubl et al., 2009). The range of $T\Delta_{47}$ for luminescent cements suggests these source fluids continued to precipitate carbonate as the Moab Tongue was exhumed to shallower depths and cooler ambient temperatures

Re-fractured luminescent veins filled with non-luminescent carbonate may signal late motion on the Moab Fault (~5 Ma; Olig et al., 1996; Trudgill, 2011) or stresses related to exhumation. The association of these late cool carbonates with the fault damage zone documents its persistent influence on fluid circulation.

6.3. Deformation bands and fluid flow

Cataclastic deformation bands are typically lower-permeability structures compared to surrounding host rock, and are commonly considered barriers to fluid flow (e.g. Antonellini et al., 1994; Eichhubl et al., 2004; Fossen and Bale, 2007; Balsamo and Storti, 2010; Ballas et al., 2015; Philit et al., 2015). Once jointed, however, deformation bands can become relatively high permeability conduits, focusing fluid migration through the host rock. We found close spatial relationships between cementation temperature and the style of structural deformation at the outcrop scale. Detailed mapping by Eichhubl

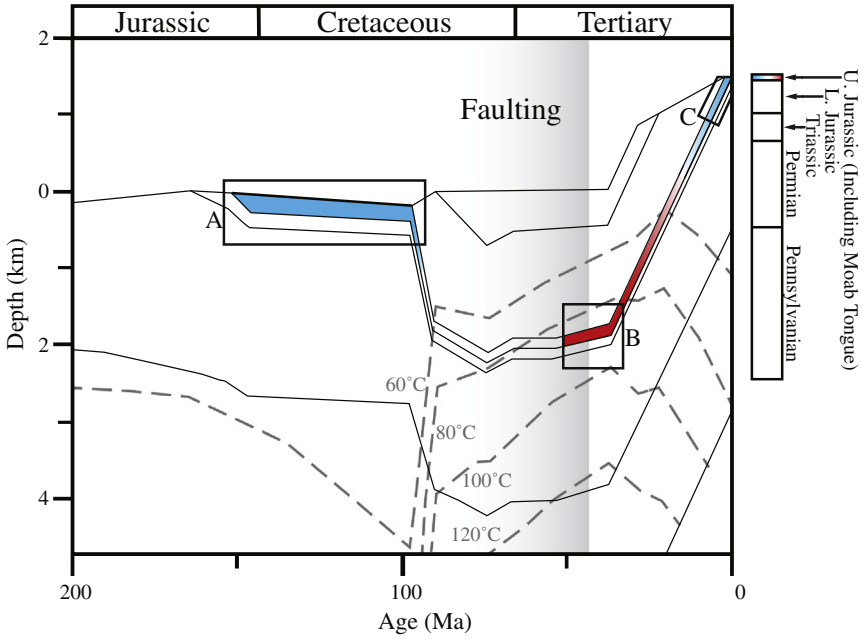

Fig. 8. Burial curve for the Paradox Basin near the study area (modified from Garden et al., 2001). Colored layer represents the Moab Tongue Sandstone, where color denotes relative temperature during burial and exhumation. Box A show timing of deformation band formation and early non-luminescent cementation. Box B indicates timing and conditions for jointing and the initiation of luminescent cementation. Box C denotes timing and conditions for the re-fracturing of cemented joints and formation of late non-luminescent cements. Gray-shaded box marks possible range of major faulting along the Moab Fault (Pevear et al., 1997; Solum et al., 2005; Trudgill, 2011). The youngest age of fault activity (ca. 43 Ma) also corresponds to known episodes of reducing fluid migration (Garden et al., 2001). (For interpretation of the references to color in this figure legend, the reader is referred to the web version of this article.)

Please cite this article as: Hodson, K.R., et al., Temperature and composition of carbonate cements record early structural control on cementation in a nascent deformation band faul..., Tectonophysics (2016), http://dx.doi.org/10.1016/j.tecto.2016.04.032

et al. (2009) demonstrated the localization of carbonate cementation around structures at CHJ. Bergman et al. (2013) identified spatial heterogeneity in the distribution of warmer and cooler carbonate, noting limited spatial distribution of the cool cements. Our new sampling expands the spatial coverage of $T\Delta_{47}$ beyond the linear transect reported by Bergman et al. (2013); Fig. 7). Our new data show that warm carbonate is found across much of the outcrop over distances of ~100 m, where it fills jointed DBn and other joints that served as conduits for the associated fluid circulation (Davatzes et al., 2005; Johansen et al., 2005; Eichhubl et al., 2009). The association of non-luminescent cements with thick and thin deformation bands suggests that these structures also influenced the distribution of fluid flow along the Moab Fault. Cool, non-luminescent carbonate occurs within and around jointed deformation bands, suggesting that associated source fluids used the fractures as preferred migration routes through the host rock. Jointed deformation bands are concentrated near the main fault strands, but also extend away from the fault zones (Fig. 7). Considering that non-luminescent carbonates formed at near-surface temperatures, it appears that deformation bands had an early influence on fault zone permeability, before substantial burial.

The timing of each style of structural deformation is clearly important to the fluid migration and cementation history of the Moab Fault. It is understood that deformation bands can form at shallow depths (e.g. Cashman and Cashman, 2000; Ballas et al., 2015), and evidence presented in this work suggests that band-parallel fractures may also form at this stage. This is interesting, as it suggests that deformation band faults can *enhance* fault zone permeability from an early stage in their development. Indeed, it appears that deformation bands precondition the rock for fracturing. Cataclasis and porosity reduction locally strengthens the rock, resulting in subsequent jointing of the stiff inclusions in a relatively soft matrix (Tindall and Eckert, 2015). Thus, paradoxically, these low-permeability features may ultimately lead to enhanced permeability of the rock, as recorded at CHJ by the distribution of early carbonate cements.

7. Conclusion

We combine clumped isotope paleothermometry with bulk C and O isotopic data and micro- to outcrop-scale structural observations to investigate carbonate cementation at Courthouse Junction along the Moab Fault. We identify carbonate populations with distinct isotopic compositions, precipitation temperatures and luminescence characteristics, each associated with different source fluid chemistries and different deformation structures. An early phase of cementation produced non-luminescent carbonate with cool precipitation temperatures in close association with the formation of deformation bands. Source fluids for the cements had isotopic compositions similar to marine waters, possibly containing dissolved limestone. Following peak burial, fractures associated with faulting and exhumation provided conduits for the circulation of meteoric waters, mixed with either an organic-carbon rich fluid or magmatic CO_2, resulting in the formation of luminescent carbonate cements at warm temperatures. The range of temperatures for luminescent carbonate suggests that it continued to form until exhumation reached near surface thermal conditions. Late forming non-luminescent carbonate forms at shallow depths during the last stages of exhumation.

The early episode of non-luminescent cementation reveals the enhancement cataclastic deformation bands can have on fluid circulation. Dilatant deformation bands are understood to enhance structure parallel flow (Antonellini et al., 1994), but cataclastic deformation bands are generally viewed as barriers in a porous sandstone (e.g. Antonellini and Aydin, 1994). Changes in these structures from low porosity bands to jointed conduits appear to happen early in the evolution of the fault zone, making them important controls on fluid flow at CHJ. Considering the complex deformation and cementation history observed at CHJ, it is clear that deformation band faults do not have a simple effect on fault zone permeability. Predictive modeling of the permeability of these structures, and related fracturing and jointing, thus requires characterization of the stress and diagenetic histories of the host rock. Here, we demonstrate the power of carbonate clumped isotope thermometry for determining environments for cementation and constraining fluid sources. Integration of these data with outcrop and petrographic observations, as well as the local burial history, allowed us to build a combined time–temperature history for deformation and diagenesis at Courthouse Junction. These data reveal the persistent influence of deformation structures from the very earliest stages of burial to the final stages of exhumation.

Acknowledgements

Acknowledgement is made to the Donors of the American Chemical Society Petroleum Research Fund (grants 53883-ND8 to JGC and 49704 to KWH), for partial support of this research. The clumped isotope laboratory at UW was established with support from NSF-EAR award 1156134 to KWH. We thank reviewers Marco Antonellini and Fabrizio Balsamo for their helpful suggestions and comments. We would also like to thank Ben Leutkemeyer for his help in the field, Alexander Lechler for his help in the field and laboratory, Andrew Schauer and Kyle Samek for their help in the laboratory, Julia Kelson for her help with clumped isotope methodology, and Charlotte Schreiber for her invaluable guidance on petrographic interpretation and thoughtful comments on the manuscript.

Appendix A. Supplementary data

Supplementary data to this article can be found online at http://dx.doi.org/10.1016/j.tecto.2016.04.032.

References

Antonellini, M., Aydin, A., 1994. Effect of faulting on fluid flow in porous sandstones: petrophysical properties. Am. Assoc. Pet. Geol. Bull. 78, 355–377. http://dx.doi.org/10.1306/8D2B1B60-171E-11D7-8645000102C1865D.

Antonellini, M.A., Aydin, A., Pollard, D.D., 1994. Microstructure of deformation bands in porous sandstones at Arches National Park, Utah. J. Struct. Geol. 16, 941–959. http://dx.doi.org/10.1016/0191-8141(94)90077-9.

Aydin, A., Johnson, A.M., 1978. Development of faults as zones of deformation bands and as slip surfaces in sandstone. Rock Friction and Earthquake Prediction, pp. 931–942.

Aydin, A., Borja, R.I., Eichhubl, P., 2006. Geological and mathematical framework for failure modes in granular rock. J. Struct. Geol. 28, 83–98. http://dx.doi.org/10.1016/j.jsg.2005.07.008.

Baedecker, M.J., Cozzarelli, I.M., Eganhouse, R.P., Siegel, D.I., Bennett, P.C., 1993. Crude oil in a shallow sand and gravel aquifer: III Biogeochemical reactions and mass balance modeling in anoxic groundwater. Appl. Geochem. 8, 569–586.

Ballas, G., Fossen, H., Soliva, R., 2015. Factors controlling permeability of cataclastic deformation bands and faults in porous sandstone reservoirs. J. Struct. Geol. 76, 1–21. http://dx.doi.org/10.1016/j.jsg.2015.03.013.

Balsamo, F., Storti, F., 2010. Grain size and permeability evolution of soft-sediment extensional sub-seismic and seismic fault zones in high-porosity sediments from the Crotone basin, southern Apennines, Italy. Mar. Pet. Geol. 27, 822–837. http://dx.doi.org/10.1016/j.marpetgeo.2009.10.016.

Balsamo, F., Storti, F., Gröcke, D., 2012. Fault-related fluid flow history in shallow marine sediments from carbonate concretions, Crotone basin, south Italy. J. Geol. Soc. Lond. 169, 613–626. http://dx.doi.org/10.1144/0016-76492011-109.Fault-related.

Balsamo, F., Bezerra, F.H.R., Vieira, M.M., Storti, F., 2013. Structural control on the formation of iron-oxide concretions and liesegang bands in faulted, poorly lithified cenozoic sandstones of the ParaÃba basin, Brazil. Bull. Geol. Soc. Am. 125, 913–931. http://dx.doi.org/10.1130/B30686.1.

Berg, S.S., Skar, T., 2005. Controls on damage zone asymmetry of a normal fault zone: outcrop analyses of a segment of the Moab fault, SE Utah. J. Struct. Geol. 27, 1803–1822. http://dx.doi.org/10.1016/j.jsg.2005.04.012.

Bergman, S.C., Huntington, K.W., Crider, J.G., 2013. Tracing paleofluid sources using clumped isotope thermometry of diagenetic cements along the Moab Fault, Utah. Am. J. Sci. 313, 490–515. http://dx.doi.org/10.2475/05.2013.03.

Bésuelle, P., 2001. Evolution of strain localisation with stress in a sandstone: brittle and semi-brittle regimes. Phys. Chem. Earth Solid Earth Geod. 26, 101–106. http://dx.doi.org/10.1016/S1464-1895(01)00032-1.

Boggs, S., Krinsley, D., 2006. Application of Cathodoluminescence Imaging to the Study of Sedimentary Rocks. Cambridge University Press, New York.

Please cite this article as: Hodson, K.R., et al., Temperature and composition of carbonate cements record early structural control on cementation in a nascent deformation band faul..., Tectonophysics (2016), http://dx.doi.org/10.1016/j.tecto.2016.04.032

Budd, D.A., Frost, E.L., Huntington, K.W., Allwardt, P.F., 2013. Syndepositional deformation features in high-relief carbonate platforms: long-lived conduits for diagenetic fluids. J. Sediment. Res. 83, 12–36. http://dx.doi.org/10.2110/jsr.2013.3.

Burgener, L., Huntington, K., Hoke, G., Schauer, A., Ringham, M., Latorre, C., Díaz, F., 2016. Variations in soil carbonate formation and seasonal bias over >4 km of relief in the western Andes (30 °S) revealed by clumped isotope thermometry. Earth Planet. Sci. Lett.

Cashman, S., Cashman, K., 2000. Cataclasis and deformation-band formation in unconsolidated marine terrace sand, Humboldt County, California. Geology 28, 111–114. http://dx.doi.org/10.1130/0091-7613(2000)28<111:CADFIU>2.0.CO;2.

Chan, M.A., Parry, W.T., Bowman, J.R., 2000. Diagenetic hematite and manganese oxides and fault-related fluid flow in Jurassic sandstones, Southeastern Utah. Am. Assoc. Pet. Geol. Bull. 84, 1281–1310.

Chan, M.A., Parry, W.T., Petersen, E.U., Hall, C.M., 2001. $^{40}Ar/^{39}Ar$ age and chemistry of manganese mineralization in the Moab and Lisbon fault systems, southeastern Utah. Geology 29, 331–334. http://dx.doi.org/10.1130/0091-7613(2001)029<0331.

Crossey, L.J., Karlstrom, K.E., Springer, A.E., Newell, D., Hilton, D.R., Fischer, T., 2009. Degassing of mantle-derived CO_2 and He from springs in the southern Colorado Plateau region — neotectonic connections and implications for groundwater systems. Bull. Geol. Soc. Am. 121, 1034–1053. http://dx.doi.org/10.1130/B26394.1.

Dale, A., John, C.M., Mozley, P.S., Smalley, P.C., Muggeridge, A.H., 2014. Time-capsule concretions: unlocking burial diagenetic processes in the Mancos Shale using carbonate clumped isotopes. Earth Planet. Sci. Lett. 394, 30–37. http://dx.doi.org/10.1016/j.epsl.2014.03.004.

Davatzes, N.C., Eichhubl, P., Aydin, A., 2005. Structural evolution of fault zones in sandstone by multiple deformation mechanisms: Moab fault, southeast Utah. Geol. Soc. Am. Bull. 117, 135. http://dx.doi.org/10.1130/B25473.1.

Defliese, W.F., Hren, M.T., Lohmann, K.C., 2015. Compositional and temperature effects of phosphoric acid fractionation on Δ47 analysis and implications for discrepant calibrations. Chem. Geol. http://dx.doi.org/10.1016/j.chemgeo.2014.12.018.

Dennis, K.J., Schrag, D.P., 2010. Clumped isotope thermometry of carbonatites as an indicator of diagenetic alteration. Geochim. Cosmochim. Acta 74, 4110–4122. http://dx.doi.org/10.1016/j.gca.2010.04.005.

Dennis, K.J., Affek, H.P., Passey, B.H., Schrag, D.P., Eiler, J.M., 2011. Defining an absolute reference frame for "clumped" isotope studies of CO_2. Geochim. Cosmochim. Acta 75, 7117–7131. http://dx.doi.org/10.1016/j.gca.2011.09.025.

Doelling, H.H., 1985. Geology of Arches National Park. Utah Geological and Mineral Survey. Salt Lake City, UT.

Eagle, R.A., Schauble, E.A., Tripati, A.K., Tütken, T., Hulbert, R.C., Eiler, J.M., 2010. Body temperatures of modern and extinct vertebrates from (13)C–(18)O bond abundances in bioapatite. Proc. Natl. Acad. Sci. U. S. A. 107, 10377–10382. http://dx.doi.org/10.1073/pnas.0911115107.

Eichhubl, P., Taylor, W.L., Pollard, D.D., Aydin, A., 2004. Paleo-fluid flow and deformation in the Aztec Sandstone at the Valley of Fire, Nevada—evidence for the coupling of hydrogeologic, diagenetic, and tectonic processes. Geol. Soc. Am. Bull. 116, 1120. http://dx.doi.org/10.1130/B25446.1.

Eichhubl, P., Davatzes, N.C., Becker, S.P., 2009. Structural and diagenetic control of fluid migration and cementation along the Moab fault, Utah. Am. Assoc. Pet. Geol. Bull. 93, 653–681. http://dx.doi.org/10.1306/02180908080.

Eichhubl, P., Hooker, J.N., Laubach, S.E., 2010. Pure and shear-enhanced compaction bands in Aztec Sandstone. J. Struct. Geol. 32, 1873–1886. http://dx.doi.org/10.1016/j.jsg.2010.02.004.

Eiler, J.M., 2007. "Clumped-isotope" geochemistry—the study of naturally-occurring, multiply-substituted isotopologues. Earth Planet. Sci. Lett. 262, 309–327. http://dx.doi.org/10.1016/j.epsl.2007.08.020.

Eiler, J.M., 2011. Paleoclimate reconstruction using carbonate clumped isotope thermometry. Quat. Sci. Rev. 30, 3575–3588. http://dx.doi.org/10.1016/j.quascirev.2011.09.001.

Fossen, H., Bale, A., 2007. Deformation bands and their influence on fluid flow. Am. Assoc. Pet. Geol. Bull. 91, 1685–1700. http://dx.doi.org/10.1306/07300706146.

Fossen, H., Schultz, R.A., Shipton, Z.K., Mair, K., 2007. Deformation bands in sandstone: a review. J. Geol. Soc. Lond. 164, 755–769. http://dx.doi.org/10.1144/0016-76492006-036.

Foxford, K.A., Garden, I.R., Guscott, S.C., Burley, S.D., Lewis, J.J.M., Walsh, J.J., Watterson, J., 1996. The field geology of the Moab Fault. Geology and Resources of the Paradox Basin: Utah Geological Association Guidebook. vol. 25, pp. 265–283.

Garden, I.R., Guscott, S.C., Burley, S.D., Foxford, K.A., Walsh, J.J., Marshall, J., 2001. An exhumed palaeo-hydrocarbon migration fairway in a faulted carrier system, Entrada Sandstone of SE Utah, USA. Geofluids 1, 195–213. http://dx.doi.org/10.1046/j.1468-8123.2001.00018.x.

Ghisetti, F., Kirschner, D.L., Vezzani, L., Agosta, F., 2001. Stable isotope evidence for contrasting paleoflud circulation in thrust faults and normal faults of the central Apennines, Italy. J. Geophys. Res. 106, 8811–8825. http://dx.doi.org/10.1029/2000jb900377.

Ghosh, P., Adkins, J., Affek, H., Balta, B., Guo, W., Schauble, E.A., Schrag, D., Eiler, J.M., 2006. $^{13}C—^{18}O$ bonds in carbonate minerals: a new kind of paleothermometer. Geochim. Cosmochim. Acta 70, 1439–1456. http://dx.doi.org/10.1016/j.gca.2005.11.014.

Gibson, R.G., 1998. Physical character and fluid-flow properties of sandstone-derived fault gouge. In: Coward, M.P., Johnson, H., Daltaban, T.S. (Eds.), Structural Geology in Reservoir Characterization, Geological Society of London Special Publication, pp. 83–97.

Graham Wall, B.R., Girbacea, R., Mesonjesi, A., Aydin, A., 2006. Evolution of fracture and fault-controlled fluid pathways in carbonates of the Albanides fold-thrust belt. Am. Assoc. Pet. Geol. Bull. 90, 1227–1249. http://dx.doi.org/10.1306/03280604014.

Guo, W., Mosenfelder, J.L., Goddard, W.A., Eiler, J.M., 2009. Isotopic fractionations associated with phosphoric acid digestion of carbonate minerals: insights from first-principles theoretical modeling and clumped isotope measurements. Geochim. Cosmochim. Acta 73, 7203–7225. http://dx.doi.org/10.1016/j.gca.2009.05.071.

Gutiérrez, F., 2004. Origin of the salt valleys in the Canyonlands section of the Colorado Plateau Evaporite-dissolution collapse versus tectonic subsidence. Geomorphology 57, 423–435. http://dx.doi.org/10.1016/S0169-555X(03)00186-7.

Hilton, D.R., Ramírez, C.J., Mora-Amador, R., Fischer, T.P., Füri, E., Barry, P.H., Shaw, A.M., 2010. Monitoring of temporal and spatial variations in fumarole helium and carbon dioxide characteristics at Poás and Turrialba Volcanoes, Costa Rica (2001–2009). Geochem. J. 44, 431–440.

Huntington, K.W., Lechler, A.R., 2015. Carbonate clumped isotope thermometry in continental tectonics. Tectonophysics 647-648, 1–20. http://dx.doi.org/10.1016/j.tecto.2015.02.019.

Huntington, K.W., Eiler, J.M., Affek, H.P., Guo, W., Bonifacie, M., Yeung, L.Y., Thiagarajan, N., Passey, B., Tripati, A., Daëron, M., Came, R., 2009. Methods and limitations of "clumped" CO_2 isotope (Delta47) analysis by gas-source isotope ratio mass spectrometry. J. Mass Spectrom. 44, 1318–1329. http://dx.doi.org/10.1002/jms.1614.

Irwin, H., Curtis, C., Coleman, M., 1977. Isotopic evidence for source of diagenetic carbonates formed during burial of organic-rich sediments. Nature 269, 209–213.

Johansen, T.E.S., Fossen, H., Kluge, R., 2005. The impact of syn-faulting porosity reduction on damage zone architecture in porous sandstone: an outcrop example from the Moab Fault, Utah. J. Struct. Geol. 27, 1469–1485. http://dx.doi.org/10.1016/j.jsg.2005.01.014.

Kim, S., O'Neil, J.R., 1997. Equilibrium and nonequilibrium oxygen isotope effects in synthetic carbonates. Geochim. Cosmochim. Acta 61, 3461–3475.

Kirschner, D.L., Kennedy, L.A., 2001. Limited syntectonic fluid flow in carbonate-hosted thrust faults of the Front Ranges, Canadian Rockies, inferred from stable isotope data and structures. J. Geophys. Res. 106, 8827. http://dx.doi.org/10.1029/2000JB900414.

Kluge, T., John, C.M., Jourdan, A.-L., Davis, S., Crawshaw, J., 2015. Laboratory calibration of the calcium carbonate clumped isotope thermometer in the 25–250 °C temperature range. Geochim. Cosmochim. Acta 157, 213–227. http://dx.doi.org/10.1016/j.gca.2015.02.028.

Knipe, R.J., Fisher, Q.J., Clennell, M.R., Farmer, A.B., Harrison, A., Kidd, B., McAllister, E., Porter, J.R., White, E.A., 1997. Fault seal analysis: successful methodologies, application and future directions. Hydrocarbon Seals: Importance for Exploration and Production: Norwegian Petroleum Society Special Publication, pp. 15–40.

Laubach, S.E., Eichhubl, P., Hilgers, C., Lander, R.H., 2010. Structural diagenesis. J. Struct. Geol. 32, 1866–1872. http://dx.doi.org/10.1016/j.jsg.2010.10.001.

Loyd, S.J., Corsetti, F.A., Eiler, J.M., Tripati, A.K., 2012. Determining the diagenetic conditions of concretion formation: assessing temperatures and pore waters using clumped isotopes. J. Sediment. Res. 82, 1006–1016. http://dx.doi.org/10.2110/jsr.2012.85.

Lucic, G., Stix, J., Wing, B., 2015. Structural controls on the emission of magmatic carbon dioxide gas, Long Valley Caldera, USA. J. Geophys. Res. Solid Earth 120, 2262–2278. http://dx.doi.org/10.1002/2014JB011760.

McCaig, A.M., Wayne, D.M., Marshall, J.D., Banks, D., Henderson, I., 1995. Isotopic and fluid inclusion studies of fluid movement along the Gavarnie Thrust, Cenral Pyrenees: reaction fronts in carbonate mylonites. Am. J. Sci. 295, 309–343.

Mook, W.G., 1986. ^{13}C in atmospheric CO_2, Netherlands. J. Sea Res. 20, 211–223.

Nelson, S.T., Davidson, J.P., Sullivan, K.R., 1992. New age determinations of central Colorado Plateau laccoliths, Utah: recognizing disturbed K–Ar systematics and re-evaluating tectonomagmatic relationships. Geol. Soc. Am. Bull. 104, 1547–1560. http://dx.doi.org/10.1130/0016-7606(1992)104<1547.

Nuccio, V.F., Condon, S.M., 1996. Burial and thermal history of the Paradox Basin, Utah and Colorado, and petroleum potential of the Middle Pennsylvanian Paradox Basin, Reston, Virginia. U.S. Geological Survey Bulletin 2000-O.

Ohtani, T., Fujimoto, K., Ito, H., Tanaka, H., Tomida, N., Higuchi, T., 2000. Fault rocks and past to recent fluid characteristics from the borehole survey of the Nojima fault ruptured in the 1995 Kobe earthquake, southwest Japan. J. Geophys. Res. Solid Earth 105, 16161–16171. http://dx.doi.org/10.1029/2000JB900086.

Olig, S.S., Fenton, C.H., McCleary, J., Wong, I.G., 1996. The earthquake potential of the Moab Fault and its relation to salt tectonics in the Paradox Basin, Utah. Geology and Resources of the Paradox Basin: Utah Geological Association Guidebook. vol. 25, pp. 251–264.

Parry, W.T., 1998. Fault–fluid composition from fluid-inclusion observations and solubilities of fracture-sealing minerals. Tectonophysics 290, 1–26. http://dx.doi.org/10.1016/S0040-1951(98)00013-4.

Pevear, D.R., Vrolijk, P.L., Lomgstaffe, F.J., 1997. Timing of Moab fault displacement and fluid movement integrated with burial history using radiogenic and stable isotopes. Geofluids II Extended Abstracts, pp. 42–45.

Philit, S., Soliva, R., Labaume, P., Gout, C., Wibberley, C., 2015. Relations between shallow cataclastic faulting and cementation in porous sandstones: first insight from a groundwater environmental context. J. Struct. Geol. 81, 89–105. http://dx.doi.org/10.1016/j.jsg.2015.10.001.

Sample, J.C., Reid, M.R., Tobin, H.J., Moore, J.C., 1993. Carbonate cements indicate channeled fluid flow along a zone of vertical faults at the deformation front of the Cascadia accretionary wedge (northwest U.S. coast). Geology 21, 507–510. http://dx.doi.org/10.1130/0091-7613(1993)021<0507.

Schauble, E.A., Ghosh, P., Eiler, J.M., 2006. Preferential formation of $^{13}C—^{18}O$ bonds in carbonate minerals, estimated using first-principles lattice dynamics. Geochim. Cosmochim. Acta 70, 2510–2529. http://dx.doi.org/10.1016/j.gca.2006.02.011.

Shackleton, N.J., 1986. Paleogene stable isotope events. Palaeogeogr. Palaeoclimatol. Palaeoecol. 57, 91–102.

Shackleton, N.J., Kennett, J.P., 1975. Palaeotemperature history of the Cenozoic and the initiation of Antarctic glaciation: oxygen and carbon isotope analysis in DSDP sites 277, 279 and 281. Deep Sea Drill. Proj. Rep. Publ. 29, 743–755. http://dx.doi.org/10.2973/dsdp.proc.29.117.1975.

Please cite this article as: Hodson, K.R., et al., Temperature and composition of carbonate cements record early structural control on cementation in a nascent deformation band faul..., Tectonophysics (2016), http://dx.doi.org/10.1016/j.tecto.2016.04.032

Shipton, Z.K., Evans, J.P., Kirschner, D., Kolesar, P.T., Williams, A.P., Heath, J., 2004. Analysis of CO_2 leakage through "low-porosity" faults from natural reservoirs in the Colorado Plateau, east-central Utah. In: Baines, S.J., Worden, R.H. (Eds.), Geological Storage of Carbon Dioxide — Geological Society Special Publication, pp. 43–58.

Solum, J.G., van der Pluijm, B.A., Peacor, D.R., 2005. Neocrystallization, fabrics and age of clay minerals from an exposure of the Moab Fault, Utah. J. Struct. Geol. 27, 1563–1576. http://dx.doi.org/10.1016/j.jsg.2005.05.002.

Spangler, L.E., Naftz, D.L., Peterman, Z.E., 1996. Hydrology, Chemical Quality, and Characterization of Salinity in the Navajo Aquifer in and Near the Greater Aneth Oil Field, San Juan County, Utah, U.S. Geological Survey Water-Resources Investigations Report. pp. 96–4155.

Tindall, S.E., 2014. Simple calculations of fluid flow across jointed cataclastic deformation bands. Mar. Pet. Geol. 57, 152–159. http://dx.doi.org/10.1016/j.marpetgeo.2014.05.016.

Tindall, S.E., Davis, G.H., 2003. Joint spacing and distribution in deformation band shear zones. Geol. Mag. 140, 1–9. http://dx.doi.org/10.1017/S0016756802007082.

Tindall, S., Eckert, A., 2015. Geometric and mechanical-stiffness controls on jointing in cataclastic deformation bands. J. Struct. Geol. 77, 126–137. http://dx.doi.org/10.1016/j.jsg.2015.05.008.

Tobin, T.S., Schauer, A.J., Lewarch, E., 2011. Alteration of micromilled carbonate $\delta^{18}O$ during Kiel Device analysis. Rapid Commun. Mass Spectrom. 25, 2149–2152. http://dx.doi.org/10.1002/rcm.5093.

Torabi, A., Fossen, H., Braathen, A., 2013. Insight into petrophysical properties of deformed sandstone reservoirs. Am. Assoc. Pet. Geol. Bull. 97, 619–637. http://dx.doi.org/10.1306/10031212040.

Tripati, A.K., Hill, P.S., Eagle, R.A., Mosenfelder, J.L., Tang, J., Schauble, E.A., Eiler, J.M., Zeebe, R.E., Uchikawa, J., Coplen, T.B., Ries, J.B., Henry, D., 2015. Beyond temperature: clumped isotope signatures in dissolved inorganic carbon species and the influence of solution chemistry on carbonate mineral composition. Geochim. Cosmochim. Acta 166, 344–371. http://dx.doi.org/10.1016/j.gca.2015.06.021.

Trudgill, B.D., 2011. Evolution of salt structures in the northern Paradox Basin: controls on evaporite deposition, salt wall growth and supra-salt stratigraphic architecture. Basin Res. http://dx.doi.org/10.1111/j.1365-2117.2010.00478.x.

Zaarur, S., Affek, H.P., Brandon, M.T., 2013. A revised calibration of the clumped isotope thermometer. Earth Planet. Sci. Lett. 382, 47–57. http://dx.doi.org/10.1016/j.epsl.2013.07.026.

Please cite this article as: Hodson, K.R., et al., Temperature and composition of carbonate cements record early structural control on cementation in a nascent deformation band faul..., Tectonophysics (2016), http://dx.doi.org/10.1016/j.tecto.2016.04.032